

Assessment of correlation energies based on the random-phase approximation

Joachim Paier,¹ Xinguo Ren,^{2,3} Patrick Rinke,^{2,3} Gustavo E. Scuseria,^{4,5} Andreas Grüneis,⁶ Georg Kresse,⁶ and Matthias Scheffler^{2,3}

¹*Institut für Chemie, Humboldt-Universität zu Berlin, Unter den Linden 6, 10099 Berlin, Germany*

²*Fritz-Haber-Institut der Max-Planck-Gesellschaft, Faradayweg 4-6, D-14195 Berlin, Germany*

³*European Theoretical Spectroscopy Facility (ETSF)*

⁴*Department of Chemistry, Rice University, Houston, Texas 77005, USA*

⁵*Department of Physics and Astronomy, Rice University, Houston, Texas 77005, USA*

⁶*Faculty of Physics and Center for Computational Materials Science, Universität Wien, Sensengasse 8/12, A-1090 Wien, Austria*

(Dated: October 22, 2018)

The random-phase approximation to the ground state correlation energy (RPA) in combination with exact exchange (EX) has brought Kohn-Sham (KS) density functional theory one step closer towards a universal, “general purpose first principles method”. In an effort to systematically assess the influence of several correlation energy contributions beyond RPA, this work presents dissociation energies of small molecules and solids, activation energies for hydrogen transfer and non-hydrogen transfer reactions, as well as reaction energies for a number of common test sets. We benchmark EX+RPA and several flavors of energy functionals going beyond it: second-order screened exchange (SOSEX), single excitation (SE) corrections, renormalized single excitation (rSE) corrections, as well as their combinations. Both the single excitation correction as well as the SOSEX contribution to the correlation energy significantly improve upon the notorious tendency of EX+RPA to underbind. Surprisingly, activation energies obtained using EX+RPA based on a KS reference alone are remarkably accurate. RPA+SOSEX+rSE provides an equal level of accuracy for reaction as well as activation energies and overall gives the most balanced performance, which makes it applicable to a wide range of systems and chemical reactions.

I. INTRODUCTION

In the context of first principles electronic structure theory “exact-exchange plus correlation in the random-phase approximation (EX+RPA)”^{1,2} has recently generated renewed and widespread interest.^{3–30} In practice, the RPA calculations are most often carried out in a non-self-consistent manner where the exchange-correlation (xc) energy contributions are evaluated with input orbitals corresponding to an approximate, usually semilocal xc energy functional. The great interest in EX+RPA is largely due to its three attractive features: (i) The exact-exchange energy (EX) cancels the spurious self-interaction error present in the Hartree energy, (ii) the RPA correlation energy is fully non-local and includes long-range van der Waals (vdW) interactions automatically and seamlessly,³¹ and (iii) EX+RPA is applicable to small-gap or metallic systems by summing up the sequence of “ring” diagrams to infinite order. The latter is in contrast to order-by-order perturbation theories [e.g. 2nd-order Møller-Plesset (MP2)]³² which break down for systems with zero gap. Moreover one can interpret the RPA as an approach that screens the non-local exchange resulting in a frequency dependent non-local screened exchange interaction, as opposed to conventional or global hybrid functionals where the parameters that reduce or “screen” the exact-exchange contribution are fixed and system independent.^{33–35} Such a system independent “screening” is expected to be unreliable for metals or wide gap insulators, where non-local exchange is almost entirely screened (metals) or prevails

to a large extent (insulators).

While a critical assessment of EX+RPA is emerging^{5–10,12–26,28} some shortcomings have been known for a while. Total energies are typically significantly overestimated,^{3,9,11,28,36,37} which is caused by an overestimation of the correlation energy at the short range. Binding energies, on the other hand, show a tendency to be underestimated.^{3,7,8,12,13,16,17,25,38} Moreover, the RPA correlation energy is not self-correlation free.^{9,37,39}

It has been demonstrated that the overestimation of the absolute correlation energy can be almost entirely removed by adding a second-order screened exchange (SOSEX) term.^{36,37,39} For one-electron systems the self-interaction error in EX+RPA is exactly canceled by adding this term,^{37,39} however, for systems with more than one electron, a many-electron self-interaction error^{40,41} prevails.³⁹ The SOSEX can also be interpreted as a correction to the RPA correlation energy that can be included to *approximately* restore the antisymmetry of the many electron description.³⁹ Furthermore, SOSEX improves binding energies, although a sizeable underestimation persists.^{9,36,37,39,42,43} The underbinding problem can also be alleviated, in particular for weakly interacting systems, by adding a correction deriving from single excitations (SE)²⁵ to EX+RPA built on a reference state obtained from Kohn-Sham (KS) density-functional theory (DFT). This suggests that RPA(+SOSEX) yields good estimations for the correlation energy but errors in the exchange energy are sizeable if Kohn-Sham orbitals are used to evaluate the exact exchange.

In light of these observations it is timely to extend the critical assessment of EX+RPA to a wider class of systems and to consider combinations of the corrections suggested before. In this paper we will address this objective by performing benchmark calculations for atomization energies on an appreciable test set of archetypal insulating solids and small molecules,^{44–47} as well as reaction and activation energies for hydrogen and non-hydrogen transfer reactions.^{48,49} The schemes we include are EX+RPA based on KS-DFT reference states, and those beyond EX+RPA by adding corrections from SE or SOSEX individually, or both of them. In addition we will also assess the hybrid-type schemes²⁵ where one replaces the total energy at the EX level evaluated with KS-DFT orbitals by that evaluated with Hartree-Fock (HF) orbitals, as an effective way to approximate the SE contribution.⁵⁰ The second-order single excitation correction can diverge when the gap between occupied and virtual states closes, with detrimental effects for the description of the transition states in chemical reactions. As briefly discussed in Ref. 25, including higher-order terms in the spirit of RPA permits a resummation of the SE correction, as will be demonstrated in Section II C. This so called renormalized SE (rSE) is well behaved and is included in our benchmark tests.

The paper is organized as follows: Sections II and III briefly summarize the important aspects of the underlying theory and the computational parameters of our work. Results on molecular and solid-state atomization energies as well as reaction energies and barrier heights are presented in Section IV before we draw conclusions in Section V.

II. THEORY

A. Basics on RPA

In order to properly position the methods applied in the present work within the formal framework of DFT, we briefly recapitulate essential equations and outline the structure of the functionals used. Currently, for total energy calculations, RPA-based functionals usually use either KS-DFT reference states, *i.e.* single-particle wavefunctions and eigenvalues or generalized KS (GKS)⁵¹ reference states to compute the *nonlocal* EX energy as well as the *nonlocal* correlation energy.^{3,5,7} Within this context, the total energy is defined as

$$E[n] = T_s[\{\phi_i\}] + E_H[n] + E_{\text{ext}}[n] + E_x[\{\phi_i\}] + E_c[\{\phi_i\}], \quad (1)$$

where the terms deriving from the potential contributions in the Hamiltonian, E_H , the electrostatic Hartree or Coulomb energy and E_{ext} , the (external) electron-ion interaction depend on the local density, whereas the last two terms, EX energy E_x and correlation energy E_c , are nonlocal contributions. Note that the KS kinetic energy, in analogy to the exact-exchange energy, is not

an explicit functional of the density, but rather of the KS orbitals. The nonlocality in E_x is due to the nonlocal exchange operator acting on each (occupied) orbital $\phi_{i\sigma}(\mathbf{r})$ associated to spin σ and its well known dependence on the (nonlocal) reduced one-particle density matrix $\rho_\sigma(\mathbf{r}, \mathbf{r}') = \sum_j^{\text{occ}} \phi_{j\sigma}(\mathbf{r})\phi_{j\sigma}^*(\mathbf{r}')$ reads

$$E_{x,\sigma} = -\frac{e^2}{2} \iint \frac{|\rho_\sigma(\mathbf{r}, \mathbf{r}')|^2}{|\mathbf{r} - \mathbf{r}'|} d^3\mathbf{r} d^3\mathbf{r}'. \quad (2)$$

In contrast to the optimized effective potential (OEP) method,^{52–54} in HF theory the exchange operator is fully nonlocal, and the action of the exchange operator on a single-particle wavefunction (*i.e.* orbital) depends on the value of that very orbital throughout the entire space (see Ref. 55). Note that the correlation energy E_c is a functional of both occupied as well as unoccupied eigenstates and requires knowledge of the associated eigenenergies as well (see below). However, both, E_x and E_c are *implicit* functionals of the electron density n (see *e.g.* Ref. 56). Recent work pursuing the construction of a *local* RPA correlation potential are presented in Refs. 57–62. Work in this direction is of great value, since it ultimately enables calculations of a self-consistent RPA correlation energies staying rigorously within the KS-DFT picture.

The RPA correlation energy can be conveniently derived from (i) perturbation theory or (ii) from the adiabatic-connection fluctuation-dissipation (ACFD) theorem.^{63–65} Fundamental to the formalism is the adiabatic connection between the Hamiltonian \hat{H} of an *interacting* many-electron system and the corresponding *noninteracting* KS Hamiltonian \hat{H}_{KS} . Formally, both systems may be simultaneously described by a coupling constant dependent Hamiltonian $\hat{H}(\lambda)$ with λ being the coupling-constant or the scaling factor in the electron-electron interaction, $v_\lambda = \lambda v(\mathbf{r} - \mathbf{r}')$. The electrons move in a λ -dependent external potential $v_{\text{ext}}^\lambda(\mathbf{r})$. Note that the ground-state density of $\hat{H}(\lambda)$ for all $\lambda \in [0, 1]$ is constant and equals the physical ground-state density $n(\mathbf{r})$, *i.e.* the ground-state density of the real system. $\hat{H}(\lambda = 1)$ is the physical many-electron Hamiltonian with $v_{\lambda=1}(\mathbf{r}) = v_{\text{ext}}(\mathbf{r})$, and $\hat{H}(\lambda = 0)$ is the KS Hamiltonian with $v_{\lambda=0}(\mathbf{r}) = v_{\text{KS}}(\mathbf{r}) = v_{\text{ext}}(\mathbf{r}) + v_H(\mathbf{r}) + v_{\text{xc}}(\mathbf{r})$. $v_H(\mathbf{r})$ is the electrostatic Hartree potential and $v_{\text{xc}}(\mathbf{r})$ is the xc potential. Within ACFD, the *exact* KS correlation energy can be written as

$$E_c = -\int_0^\infty \frac{du}{2\pi} \int_0^1 d\lambda \int d\mathbf{r} \int d\mathbf{r}' \{ \nu(\mathbf{r} - \mathbf{r}') \times (\chi_\lambda(\mathbf{r}, \mathbf{r}'; iu) - \chi_0(\mathbf{r}, \mathbf{r}'; iu)) \}. \quad (3)$$

Here $\nu(\mathbf{r} - \mathbf{r}') = 1/|\mathbf{r} - \mathbf{r}'|$ is the bare Coulomb interaction kernel, and χ_0 is the KS independent-particle response function at imaginary frequencies iu ,

$$\chi_0(\mathbf{r}, \mathbf{r}'; iu) = 2 \sum_i^{\text{occ}} \sum_a^{\text{unocc}} \frac{\phi_i^*(\mathbf{r})\phi_a(\mathbf{r})\phi_a^*(\mathbf{r}')\phi_i(\mathbf{r}')}{iu + \varepsilon_i - \varepsilon_a} + c.c., \quad (4)$$

where *c.c.* denotes “complex conjugate” and the prefactor 2 accounts for the spin-degeneracy in closed-shell systems. In Eq. (3), χ_λ is the density-density response function of the “intermediately” interacting many-electron system employing a scaled Coulomb potential ν_λ . We adhere to the commonly used notation of $i, j \dots$ being occupied, *i.e.* hole KS states and $a, b \dots$ being unoccupied or virtual, particle states. In principle, a Dyson-type integral equation⁶⁶ has to be solved for χ_λ ,

$$\chi_\lambda = \chi_0 + \chi_0 (\nu_\lambda + f_{xc}^\lambda) \chi_\lambda, \quad (5)$$

with f_{xc}^λ as the xc kernel, *i.e.* the functional derivative of the exchange-correlation potential with respect to the density. Within RPA, $f_{xc} = 0$, *i.e.* using many-body terminology,⁶⁷ so-called vertex corrections are not included in the response function χ or equivalently in the screening of the Coulomb interaction. Solving Eq. (5) for χ_λ with $f_{xc}^\lambda = 0$ corresponds to the diagrammatic resummation of ring graphs^{36,68} to infinite order. In passing we note that, working within RPA, Eq. (5) can be rearranged to

$$\chi_\lambda = (1 - \chi_0 \nu_\lambda)^{-1} \cdot \chi_0 = [1 + \chi_0 \nu_\lambda + \chi_0 \nu_\lambda \chi_0 \nu_\lambda + \dots] \cdot \chi_0, \quad (6)$$

reflecting the above mentioned summation of the (screened) Coulomb interaction up to infinite order in $\chi_0 \nu_\lambda$. As will be seen later, Eq. (6) resembles the coupled-cluster amplitude equations where so-called particle-particle, particle-hole, and hole-hole ladder terms have been removed (see Eq. 17). Starting from Eq. (6), the λ -integral is readily done and the final expression for the RPA correlation energy reads

$$E_c^{\text{RPA}} = \int_0^\infty \frac{du}{2\pi} \text{Tr}\{\ln(1 - \chi_0(iu)\nu) + \chi_0(iu)\nu\}. \quad (7)$$

B. From coupled-cluster theory to RPA and RPA+SOSEX

From a DFT purist’s point of view, the previously outlined ACFD terminology for the RPA is certainly the most consistent way to classify “RPA” as a correlation energy *functional* to the many-electron ground-state. An alternative formulation of the RPA may be motivated starting from many-body theory. Many-body or equivalently field-theoretical diagrammatic techniques originally developed in quantum electrodynamics and nuclear physics⁶⁹ have been applied to the homogeneous electron gas as well as finite systems like atoms and molecules for several decades already. For systems that are not strongly correlated, the most successful diagrammatic, partial summation technique (see Refs. 56 and 70) is the coupled cluster (CC) expansion of the many-electron wavefunction. The CC expansion to the homogeneous electron gas has been applied by Freeman,³⁶ Kümmel, Lührmann, and Zabolitzky,⁷¹ as well as Bishop and Lührmann.^{72,73} The same CC expansion techniques

are indispensable ingredients for highly accurate molecular calculations. Here, pioneers have been Čížek,^{74,75} Paldus *et al.*,⁷⁶ and Bartlett and Purvis⁷⁷ to name a few. A more complete list of references may be found in the recent review article by Bartlett and Musiał.⁷⁰

The CC expansion relies on the ansatz for the many-electron wavefunction, $|\Psi\rangle$,

$$|\Psi\rangle = e^{\hat{T}} |\Phi\rangle, \quad (8)$$

to generate the exact ground state from the ground state $|\Phi\rangle$ of the reference system commonly within the HF approximation. Note that \hat{T} may be represented by a sum of single, double, and higher-order excitation operators, generating in a similar way to configuration interaction (CI) techniques, singly, doubly substituted determinants based on the HF reference wavefunction $|\Phi\rangle$. However, the CC expansion is distinct from CI by virtue of the exponential ansatz used in CC expansions (Eq. 8) for the wavefunction $|\Psi\rangle$, with

$$e^{\hat{T}} = 1 + \hat{T} + \frac{1}{2!} \hat{T}^2 + \frac{1}{3!} \hat{T}^3 + \dots, \quad (9)$$

introducing so-called disconnected products of excitations responsible for the size-extensivity of the coupled cluster correlation energy.⁷⁸

In coupled-cluster doubles theory (CCD) the excitation operator corresponds to a double excitation operator only, where

$$\hat{T} \equiv \hat{T}_2 \quad \text{with} \quad (10)$$

$$\hat{T}_2 |\Phi\rangle = \sum_{i<j}^{N_{\text{occ.}}} \sum_{a<b}^{N_{\text{virt.}}} t_{ij}^{ab} |\Phi_{ij}^{ab}\rangle. \quad (11)$$

The amplitudes t_{ij}^{ab} are obtained from solving a set of so-called doubles amplitude equations reading

$$\langle \Phi_{ij}^{ab} | e^{-\hat{T}} \hat{H} e^{\hat{T}} | \Phi \rangle = 0. \quad (12)$$

Solving Eq. (12) self-consistently for t_{ij}^{ab} results in a resummation of infinitely many diagrams of a certain type. Removing all terms from the above amplitude equation that do not correspond to so-called ring-diagrams defines the so-called ring-CCD.

Recently, the equivalence between direct, *i.e.* “Coulomb term only” ring-CCD (drCCD) and RPA as considered by Freeman,³⁶ reexamined by Grüneis and Kresse⁴³ and Scuseria *et al.*,⁶ has been demonstrated. Scuseria *et al.* algebraically showed that the CCD approximation to the many-electron wavefunction contains the ring-approximation, *i.e.* the RPA to the ground-state correlation energy, but also includes selected higher-order exchange and ladder diagrams.^{36,72,73} In other words, RPA equals drCCD and therefore corresponds to a subset of CCD diagrams.

Within the framework of CC expansions, the RPA and RPA+SOSEX correlation energies may be calculated using drCCD amplitudes $\{t_{ij}^{ab}\}$ by employing the respective

equations,^{6,36,37}

$$E_c^{\text{RPA}} = \frac{1}{2} \sum_{ijab} B_{ia,jb}^* t_{ij}^{ab} \quad (13)$$

$$E_c^{\text{RPA+SOSEX}} = \frac{1}{2} \sum_{ijab} K_{ia,jb} t_{ij}^{ab}. \quad (14)$$

The matrices $B_{ia,jb}$ and $K_{ia,jb}$ are of rank $N_{\text{occ}} \times N_{\text{virt}}$, and they are defined by two-electron integrals $B_{ia,jb} = \langle ij | ab \rangle$ and $K_{ia,jb} = \langle ij | ab \rangle - \langle ij | ba \rangle$, respectively,

$$\langle pq | rs \rangle = \iint \phi_p^*(\mathbf{x}) \phi_r(\mathbf{x}) \frac{1}{|\mathbf{r} - \mathbf{r}'|} \phi_q^*(\mathbf{x}') \phi_s(\mathbf{x}') d\mathbf{x} d\mathbf{x}', \quad (15)$$

with $\mathbf{x} = \{\mathbf{r}, \sigma\}$. The amplitudes $\{t_{ij}^{ab}\}$ are obtained from solving a set of nonlinear Riccati equations, closely related to the time-dependent HF or more precisely the time-dependent Hartree method,⁶

$$\begin{aligned} \langle ij | ab \rangle + (\varepsilon_c - \varepsilon_k) \delta_{ac} \delta_{ik} t_{kj}^{cb} + \langle ic | ak \rangle t_{kj}^{cb} \\ + t_{ik}^{ac} (\varepsilon_c - \varepsilon_k) \delta_{bc} \delta_{jk} + t_{kj}^{cb} \langle ic | ak \rangle \\ + t_{ik}^{ac} \langle kl | cd \rangle t_{lj}^{db} = 0. \end{aligned} \quad (16)$$

The previous equation can be rewritten in a more compact form,⁶

$$\mathbf{B} + \mathbf{AT} + \mathbf{TA} + \mathbf{TBT} = 0, \quad (17)$$

with $A_{ia,jb} = (\varepsilon_a - \varepsilon_i) \delta_{ij} \delta_{ab} + \langle ib | aj \rangle$, $B_{ia,jb} = \langle ij | ab \rangle$, and $T_{ia,jb} = t_{ij}^{ab}$, underlining the quadratic order in the amplitudes' matrix \mathbf{T} .

Freeman has evaluated the RPA correlation energy of the unpolarized electron gas for various electron densities³⁶ using the drCCD equations and compared them to Hedin's RPA results (see Table II in Ref. 79) following an approach suggested by Nozières and Pines.⁸⁰

Both agree to within the numerical accuracy employed in the calculations. Moreover, Freeman has gone beyond RPA via inclusion of the second-order screened exchange (SOSEX) diagram. He found that SOSEX reduces the correlation energy by about 30%. Monkhorst and Oddershede came to similar conclusions employing RPA and RPA+SOSEX to metallic hydrogen,⁸¹ and Grüneis observed a similar reduction of the correlation energy for small atoms³⁷ finding good agreement with highly accurate coupled cluster correlation energies only after inclusion of SOSEX. Finally we note that until recently the formulation of SOSEX within an ACFD framework has not been entirely clear, but has lately been shown by Jansen *et al.*⁸²

C. Single excitations and their renormalization

As alluded to above, in most practical calculations, RPA and SOSEX correlation energies are evaluated using KS orbitals from local or semilocal density functionals,^{3,12} or generalized KS orbitals^{7,9,17} from

range-separated density functionals. This way, both RPA and SOSEX can be interpreted in terms of many-body perturbation theory (MBPT) based on a (generalized) KS reference state, where only a selected type of diagrams are summed up to infinite order. If one performs a simple Rayleigh-Schrödinger perturbation theory (RSPT) starting from an (approximate) KS-DFT reference, and examines the perturbation series at second order, one can identify a term arising from single excitations (SE), that is not included in RPA or SOSEX correlation energies. In terms of single-particle orbitals, this term can be expressed as

$$E_c^{\text{SE}} = \sum_{ia} \frac{|\langle i | v^{\text{HF}} - v^{\text{eff}} | a \rangle|^2}{\varepsilon_i - \varepsilon_a}, \quad (18)$$

where v^{HF} is the self-consistent HF potential, and v^{eff} is the effective single-particle potential that defines the non-interacting reference Hamiltonian h^{eff} giving rise to the single-particle orbitals $|i\rangle$ and $|a\rangle$ in the above expression. (See the supplemental material of Ref. 25 for a detailed derivation.) As is obvious from Eq. (18), E_c^{SE} trivially vanishes for the HF reference, *i.e.*, when $v^{\text{eff}} = v^{\text{HF}}$, but is nonzero otherwise. It has been shown that adding this term to RPA improves the description of weak interactions significantly.²⁵ Note that the choice of v^{eff} in Eq. (18) is slightly different in RSPT from that in the 2nd-order Görling-Levy perturbation theory (GL2).⁸³ In the latter case, $v^{\text{eff}} = v^{\text{EXX-OEP}}$, with $v^{\text{EXX-OEP}}$ being the exact-exchange OEP⁵²⁻⁵⁴ potential. The difference of the two perturbation theories lies in the choice of the adiabatic-connection path (λ -integral) – in GL2 the electron density is kept fixed along the path way and the perturbative Hamiltonian has a non-linear dependence on λ , whereas in RSPT the λ -dependence of the perturbative Hamiltonian is linear, but the electron density varies along the λ -integral. Eq. (18) in RSPT is more efficient and practically useful in the sense that there is no need to solve the computationally intensive and sometimes numerically problematic EXX-OEP equation and more flexible in the sense that it can be matched to any suitable reference state. The price one has to pay is that the theory, strictly speaking, is not KS-DFT formulated within the ACFD framework.

The SE contribution at second order as given by Eq. (18) may become ill-behaved when the single-particle gap closes. To deal with this problem, in Ref. 25 a sequence of higher-order terms involving SE processes have been identified and summed up in the spirit of RPA. This leads to a “renormalized” SE (rSE) contribution to the correlation energy,

$$E_c^{\text{rSE}} = \sum_{ia} \frac{|\langle i | \Delta v | a \rangle|^2}{\varepsilon_i - \varepsilon_a + \langle i | \Delta v | i \rangle - \langle a | \Delta v | a \rangle}, \quad (19)$$

where $\Delta v = v^{\text{HF}} - v^{\text{eff}}$. The additional term $\langle i | \Delta v | i \rangle - \langle a | \Delta v | a \rangle$ in the denominator of Eq. (19) is negative definite, and prevents the possible divergence of the ex-

TABLE I: The list of methods used throughout this work and their acronyms. Note that the total energy at the exact-exchange level is abbreviated by “EX”.

(EX+RPA)@PBE	EX and RPA evaluated with a PBE reference, <i>i.e.</i> PBE orbitals and eigenvalues
HF+RPA@PBE	HF total energy combined with RPA using a PBE reference
(EX+RPA+SE)@PBE	EX and RPA augmented with SE using the PBE reference
(EX+RPA+rSE)@PBE	EX and RPA augmented with rSE using the PBE reference
HF+(RPA+SOSEX)@PBE	HF total energy combined with RPA+SOSEX using the PBE reference
(EX+RPA+SOSEX)@PBE	EX, RPA+SOSEX using the PBE reference
(EX+RPA+SOSEX+rSE)@PBE	EX, RPA+SOSEX, and rSE using the PBE reference

pression even when the KS gap closes. The rSE correction is therefore expected to have a more general applicability, while preserving the good performance of the 2nd-order SE for wide-gap molecules and insulators. In deriving Eq. (19), however, the “non-diagonal” elements in the higher-order SE diagrams have been neglected for simplicity. Such an approach lacks invariance with respect to unitary transformations (orbital rotations) within the occupied and/or unoccupied subspaces. The orbital-rotation-invariance can be restored by including also the “non-diagonal” elements. This can be achieved by first semi-diagonalizing the Fock Hamiltonian $f = h^{\text{eff}} + v^{\text{HF}} - v^{\text{eff}}$ separately within the occupied and unoccupied subspaces of h^{eff} and utilizing the resultant (so-called *semi-canonical*) orbitals and orbital energies in Eq. (18). A detailed description of this procedure will be presented in a forthcoming paper. However, we emphasize that results presented in this work are based on Eq. (19), but despite the lack of rotational invariance in the orbitals of this approach, numerical results are only very little affected.

As also demonstrated in Ref. 25, the SE contributions to the correlation energy can be effectively accounted for to a large extent by replacing the non-self-consistent HF total energy computed using KS orbitals by its self-consistent counterpart. In this so-called hybrid-RPA scheme the RPA correlation energy is still evaluated using KS orbitals, whereas the EX term is evaluated using HF orbitals. The same strategy can be applied to “RPA+SOSEX” calculations. In this work, we will benchmark the influence of SE contributions on the performance of RPA and SOSEX both by explicitly including the (r)SE corrections and in terms of the hybrid scheme.

As outlined in Ref. 25 by Ren *et al.*, rendering the energy functional stationary with respect to variations in the orbitals implies a zero correlation energy contribution stemming from SEs. This is well known as Brillouin’s theorem. It will be demonstrated in this work, that SE effects represent a non-negligible contribution to the correlation energy and consequently affect results on thermochemistry and kinetics. In the field of quantum chemistry effects induced by SEs are known as orbital-relaxation effects.^{84,85} Besides MBPT discussed above, the SE terms are present in the CC theory as well. In this

context, Scuseria and Schaefer have shown that CCD employing optimized-orbitals (see Ref. 86) gives results very close to CCSD. On the other hand, optimizing orbitals for CCSD calculations does not lead to significant improvements in the wavefunction. In other words, changes in the correlation energy induced upon inclusion of SEs may be effectively incorporated by means of a unitary transformation, *i.e.* rotation of the orbitals, as given in Eq. (6) of Ref. 86.

We close this section by presenting Table I, which summarizes the acronyms of the various methods applied in this work. For the KS single-determinant reference wave function we use the Perdew, Burke, and Ernzerhof (PBE)⁸⁷ generalized gradient approximation (GGA). We adopt the notation introduced by Ren *et al.* in Ref. 17, hence “@PBE” means “evaluated using PBE orbitals and orbital energies”. This particular choice of orbitals is mainly driven by the following arguments: (i) PBE contains no empirically adjusted parameters, (ii) performs slightly better than LDA (see *e.g.* Ref. 12), and (iii) it is computationally less expensive to calculate the orbitals using semilocal functionals instead of *e.g.* hybrid functionals.¹⁷ In addition, once one restricts the input orbitals to KS orbitals, results have shown to be virtually identical to those obtained using PBE orbitals.^{24,88}

III. COMPUTATIONAL DETAILS

Computational results of the present work are based on calculations using (i) the Vienna *ab initio* simulation package VASP,^{89–91} (ii) a development version of the GAUSSIAN⁹² suite of programs, and (iii) FHI-aims.^{93,94} All of the software packages used have the RPA and RPA+SOSEX functionals available since recently.^{7,9,12,17} VASP uses periodic boundary conditions and projector augmented plane waves as a basis set, which makes it ideally suited for extended, crystalline systems. GAUSSIAN is based on local, analytic Gaussian type (GT) basis functions using open boundary conditions and the linear combination of atomic orbitals to expand the molecular orbitals. FHI-aims primarily uses numeric, atom-centered basis functions, but GT orbitals can be employed as well. In both cases, all the required integrals are evaluated numerically on an overlapping atom-centered grid.⁹³ The

resolution-of-identity approximation is used to handle the four-centered Coulomb repulsion integrals and the KS response function (details of the implementation have been presented in Ref. 94). In this work GT orbitals are used in FHI-aims calculations to facilitate a direct comparison with GAUSSIAN and the extrapolations to the complete basis set (CBS) limit.

In this work we present statistical errors for the G2-1 set,^{44–47} as well as for BH6,⁹⁵ HTBH38/04, and NHTBH38/04 sets of 38 hydrogen transfer and 38 non-hydrogen transfer barrier heights after Zhao *et al.*^{48,49} Results for the molecular test sets use a two-point extrapolation procedure on the correlation energies to attain the complete basis set (CBS) limit.^{96–98} The chosen ansatz is motivated by an atomic partial wave expansion of the two-particle many-body wavefunction,⁹⁷

$$E_{\text{corr}}^X = E_{\text{corr}}^\infty + \frac{a}{X^3}, \quad (20)$$

where the E_{corr}^X are correlation energies corresponding to the cc-pVXZ basis sets. For G2-1, CBS calculations are based on Dunning’s correlation-consistent cc-pVQZ and cc-pV5Z basis sets.^{99,100} Note that throughout this work CBS extrapolation will be denoted by, e.g., cc-pV(Q,5)Z.

Moreover, G2-1 calculations employ the Boys-Bernardi counterpoise correction¹⁰¹ to correct for basis set superposition errors (BSSE) within a particular basis set. Therefore, we emphasize that the CBS procedure uses BSSE free correlation energies. In order to avoid inaccuracies from numerical quadrature of xc energy contributions, GAUSSIAN calculations use a grid of 400 radial shells and 770 angular points in each shell to converge the KS orbitals. GAUSSIAN employs a root-mean-square convergence criterion for the density matrix in the SCF iteration of 0.1 $\mu\text{Hartree}$, which implies an energy convergence no worse than at least 0.01 $\mu\text{Hartree}$ (GAUSSIAN keyword: SCF=tight). In FHI-aims the grid setting “tight” together with “radial_multiplier=6” has been used to achieve convergence within one $\mu\text{Hartree}$.

TABLE II: Matching radii r_c of the PAW potentials used in the present work. If the matching radii differ for specific quantum numbers, they are specified for each l -quantum number using subscripts.

Valence	r_c [a.u.]	Valence	r_c [a.u.]
H 1s	1.0 _s 1.1 _{pd}	F 2s2p	1.1 _s 1.4 _{pd}
Li 1s2s	1.2 _s 1.5 _{pd}	Mg 2p3s	2.0 _{sd} 1.6 _p
B 2s2p	1.5 _s 1.7 _{pd}	Al 3s3p	1.9 _{spd} 2.0 _f
C 2s2p	1.2 _s 1.5 _{pd}	Si 3s3p	1.5 _s 1.9 _{pd}
N 2s2p	1.3 _s 1.5 _{pd}	P 3s3p	1.9 _{sp} 2.0 _{df}
O 2s2p	1.2 _s 1.5 _{pd}	Cl 3s3p	1.7 _s 1.9 _{pdf}

Results on barrier heights in BH6, HTBH38/04, and NHTBH38/04 use a cc-pV(T,Q)Z CBS extrapolation of the correlation energies and do not employ counterpoise corrections. To test for the errors incurred, we compare with benchmark results obtained using RPA and

TABLE III: Experimental lattice constants, a^{exp} , extrapolated to 0 K. Energy cutoffs for the one-electron wave functions E_{PW} as well as energy cutoffs for representing the overlap charge densities E_χ employed in the calculation of the atomization energies of solids. The corresponding structures are denoted using the Strukturbericht symbols in parenthesis in the first column (A4=diamond, B1=rock-salt, B3=zinc-blende). All energies and lattice constants in eV and \AA , respectively.

	a^{exp}	E_{PW}	E_χ
C (A4)	3.567 ^a	550	400
Si (A4)	5.430 ^a	450	300
SiC (B3)	4.358 ^a	550	400
BN (B3)	3.607 ^b	550	400
BP (B3)	4.538 ^b	450	350
AlN (B3)	4.380 ^c	550	400
AlP (B3)	5.460 ^b	450	350
LiH (B1)	4.064 ^d	600	450
LiF (B1)	4.010 ^a	600	450
LiCl (B1)	5.106 ^a	600	450
MgO (B1)	4.207 ^a	600	450

^aRef. 103, ^bRef. 104, ^c Ref. 105, ^d Ref. 106.

RPA+SOSEX given in Ref. 9. The statistical errors in barrier heights deviate from the aforementioned benchmark values by at most 1 kJ/mol. Hence, the errors incurred using smaller basis sets are minute and consequently are not expected to bias the conclusions.

The test set on atomization energies for crystalline solids includes 11 archetypal semiconductors and insulators. Specifically it comprises C, Si, SiC, BN, BP, AlN, AlP, LiH, LiF, LiCl, and MgO. The projector augmented wave (PAW) pseudopotentials (technical details in Tab. II) and kinetic energy cutoffs employed in the present calculations are identical to the ones used in Ref. 102. Table III summarizes the lattice constants used in “post-RPA” calculations. Moreover, we specify plane wave cutoffs for the overlap charge densities described in Refs. 38 and 102. The SOSEX correlation energy was calculated using a $(3 \times 3 \times 3)$ Γ -centered k mesh, except for BN and BP due to a slower k -point convergence of the energy. For these systems a $(4 \times 4 \times 4)$ mesh was used. RPA correlation energies are taken from the literature (see Ref. 38). In VASP, atoms are calculated using a supercell approach. The dimension of the supercells has been chosen as $(9 \times 9 \times 9)$ \AA^3 in size. To reduce the computational cost of the “RPA+SOSEX” calculations for isolated atoms, natural orbitals obtained using second order perturbation theory have been employed. As outlined in Ref. 107, natural orbitals substantially improve convergence of the correlation energy with respect to the number of virtual orbitals.

To assess the codes used in this work, we compare numerical results obtained using the “RPA” and “RPA+SOSEX” implementations of GAUSSIAN and FHI-aims. Table IV shows correlation energies for the He atom obtained using the cc-pV5Z basis set. In order

TABLE IV: Benchmark calculations for atomic He using FHI-aims and GAUSSIAN and a cc-pV5Z GT orbital basis set. Results are given in Hartree atomic units.

He / cc-pV5Z	GAUSSIAN	FHI-aims
HF	-2.86162468	-2.86162483
MP2	-0.03640606	-0.03640651
RPA@HF	-0.06524488	-0.06524570
(RPA+SOSEX)@HF	-0.03262244	-0.03262285

to avoid errors caused by numerical integration, we decided to use (restricted, *i.e.* spin-unpolarized) HF orbitals and eigenvalues for the calculation of RPA and RPA+SOSEX. The agreement found is close to perfect. Differences between results are within a sub-micro-Hartree error margin. In passing we mention that FHI-aims employs the resolution-of-identity (RI) technique,⁹⁴ which (i) reduces the computational workload significantly and (ii), as shown in Tab. IV, does not sacrifice accuracy. For the molecular test sets, we always cross-check the “RPA” and “RPA+SOSEX” results obtained with the GAUSSIAN suite of program and FHI-aims to make sure that the results presented in this work are not affected by the actual implementations. “SE” and “rSE” have so far only been implemented in FHI-aims and we use these results throughout.

IV. RESULTS AND DISCUSSION

Central findings of this work are summarized in Tab. V presenting binding energies in molecules (G2-1) and solids, HT activation energies or barrier heights (BH6, HTBH38) as well as NHT barrier heights (NHTBH38). Whenever results are compared to experiment or to the best theoretical estimates, we use mean error (ME) and mean unsigned error (MUE) as statistical measures to assess the accuracy of individual methods employed. Note that the experimental reference values are corrected for zero point effects and are taken from the literature (G2-1: Ref. 108; atomization energies in solids: Ref. 109; barrier heights in BH6, HT/NHTBH38: Refs. 95, 48, and 49). Reaction energies, as presented in Table VI, are calculated from barrier heights in HTBH38 and NHTBH38, respectively.

A. Atomization energies of small molecules and solids

The notorious underbinding of (EX+RPA)@PBE in molecules and solids has already been demonstrated in many studies.^{3,9,12,13,17,37,38} Table V presents MEs and MUEs in binding (atomization) energies obtained using (EX+RPA)@PBE for insulating solids (see Sec. III) as well as for the molecules contained in the G2-1 set.

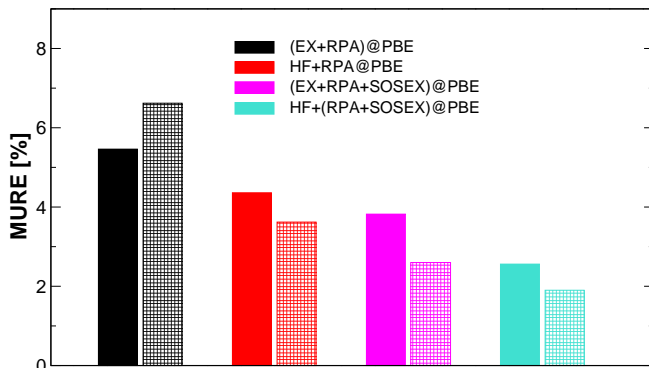


FIG. 1: Mean unsigned relative errors (MURE) in the atomization energies of 55 small molecules contained in G2-1 (full bars) and 11 insulating solids (squared bars) obtained using four of the RPA-based methods presented in this work.

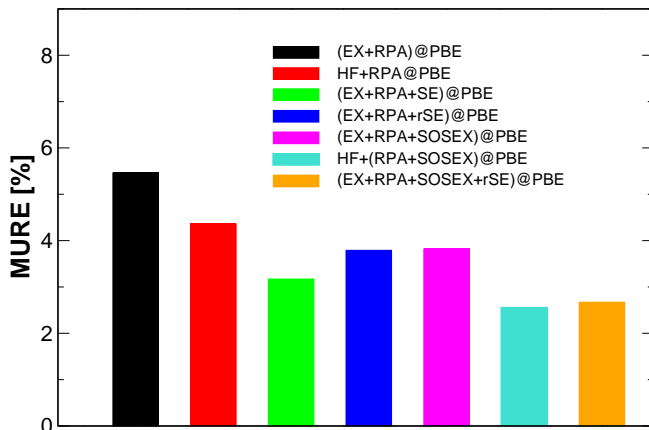


FIG. 2: Mean unsigned relative errors (MURE, given in %) in G2-1 for all RPA-based methods presented in this work. Atomization energies use counterpoise correction and correlation energies are CBS extrapolated using cc-pV(Q,5)Z.

On average, (EX+RPA)@PBE underbinds solids compared to experiment by -67 kJ/mol (see also Ref. 38) and molecules by -43 kJ/mol. We repeat that experimental binding energies are corrected for zero-point effects and are taken from the literature (for G2-1, see Ref. 108, for the test set on solids see Ref. 109 and references therein).

Following the suggestion of Ren *et al.*,²⁵ effects incurred by replacing the EX@PBE reference energy by the HF total energy have been checked for both molecules and solids. Indeed, HF+RPA@PBE improves binding energies of molecules *and* solids by almost 50% compared to (EX+RPA)@PBE. Fig. 1 presents mean unsigned *relative* errors (MURE) in molecular (full bars) as well as solid state (squared bars) binding energies. Overall differences in MUREs are rather small. For the commonly applied (EX+RPA)@PBE method, the MURE is found to be approximately 6%. Using HF at the exact exchange level reduces the MURE by more than 1%. It appears that the aforementioned improvements are less pronounced at the relative scale, and the error reduction

TABLE V: Mean errors (ME) and mean unsigned errors (MUE) in atomization or binding energies of 11 solids (see Tab. III) and 55 molecules (G2-1), in the barrier heights comprised in BH6, in HTBH38/04 (hydrogen transfer barriers), as well as in NHTBH38/04 (non-hydrogen transfer barriers). Results are given in kJ/mol.

Method	Solids		G2-1		BH6		HTBH38		NHTBH38	
	ME	MUE	ME	MUE	ME	MUE	ME	MUE	ME	MUE
(EX+RPA)@PBE	-67.5	67.5	-42.7	42.8 ^a	1.2	7.5 ^a	-0.8	7.1	-10.5	12.1
HF+RPA@PBE	-34.7	36.7	-25.3	30.3	-25.5	25.5	-36.8	36.8	-48.5	48.5
(EX+RPA+SE)@PBE			-14.2	22.9	-23.8	23.8	-52.7	52.7	-50.6	51.9
(EX+RPA+rSE)@PBE			-26.2	27.4	-14.8	16.3	-18.0	21.7	-31.4	31.4
(EX+RPA+SOSEX)@PBE	-27.0	27.0	-20.3	23.0 ^a	17.6	17.6 ^a	22.2	22.2	13.4	15.5
HF+(RPA+SOSEX)@PBE	5.8	17.4	-2.9	13.0	-9.2	9.2	-13.8	13.8	-24.7	25.5
(EX+RPA+SOSEX+rSE)@PBE			-4.0	13.9	3.1	3.7	3.6	5.4	-6.3	17.6

^a See Ref. 9. Note that differences in the MUE of G2-1 are due to the different values for the experimental dissociation energies (see Ref. 108).

is apparently bigger for solids than for molecules.

The explicit inclusion of the SE contribution to the correlation energy “SE@PBE” obtained using Eq. (18) has been evaluated for molecules only. Adding “SE@PBE” to (EX+RPA)@PBE results in an ME of approximately -14 kJ/mol (see Tab. V) and an MUE of approximately 23 kJ/mol, clearly outperforming HF+RPA@PBE. Relative unsigned errors in G2-1 collected in Fig. 2 further corroborate the improvements of (EX+RPA+SE)@PBE over HF+RPA@PBE. Overall, these results confirm the findings presented by Ren *et al.* in Ref. 25. However, “Renormalization” of the SE contributions, as required for systems with a small one-electron band gap in PBE (see activation energies discussed in Sec. IV B) brings the atomization energies in the G2-1 test set back into almost perfect agreement with HF+RPA@PBE. Therefore, the good agreement with experiment for the G2-1 test set on the level of (EX+RPA+SE)@PBE is most likely to some extent fortuitous.

As extensively discussed in Refs. 37 and 9, the (RPA+SOSEX) correlation energy, here denoted as “(RPA+SOSEX)@PBE,” represents a correction to (EX+RPA)@PBE rectifying the one-electron self-interaction error contained in “RPA@PBE” due to exclusion principle violating diagrams.³⁹ Results for G2-1 obtained using (EX+RPA+SOSEX)@PBE are taken from Ref. 9 and included in Tab. V. The ME in G2-1 obtained using (EX+RPA+SOSEX)@PBE is approximately equal to -20 kJ/mol. For solids, the ME error reduces to -27 kJ/mol. Compared to (EX+RPA)@PBE, this represents substantial improvements of approximately 50% for atomization energies.

Given that both SOSEX and rSE, or alternatively replacing EX@PBE by HF, alleviate the tendency of (EX+RPA)@PBE to underbind, both schemes are expected to work cooperatively for the atomization energies of small molecules. Indeed, replacing “EX@PBE” in (EX+RPA+SOSEX)@PBE by the HF total energy yields excellent results, with a slight underbinding for molecules (ME = -2.9 kJ/mol), and a slight overbinding for solids (ME=5.8 kJ/mol). Again, the

HF+(RPA+SOSEX)@PBE (ME = -2.9 kJ/mol) and the (EX+RPA+SOSEX+rSE)@PBE methods (ME = -4.0 kJ/mol) perform almost on par for molecules.

In summary, single excitation diagrams improve (EX+RPA)@PBE atomization energies of small molecules at virtually zero additional computational cost. However, as we will see below, this method fails when the one-electron band gaps in PBE become small. The better founded rSE does not perform equally well for atomization energies when comined with RPA. Combined with RPA+SOSEX it yields impressive atomization energies that are also in almost perfect agreement with the “hybrid variants” *e.g.* the (self-consistent) HF total energy together with “(RPA+SOSEX)@PBE”. Overall this indicates that (EX+RPA+SOSEX+rSE)@PBE or HF+(RPA+SOSEX)@PBE are the methods of choice for atomization energies.

B. Activation energies in HTBH38 and NHTBH38 chemical reactions

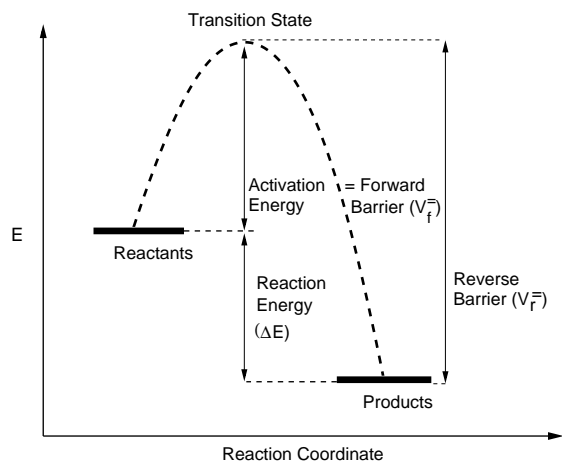


FIG. 3: Schematic of activation and reaction energies.

The ability to accurately describe the topology of multidimensional potential energy surfaces spanned by the internal molecular degrees of freedom, *i.e.* the reaction coordinates, in the course of a chemical reaction, is central to first principles electronic structure methods. Calculating the energy difference between reactants and transition states (see Fig. 3) is a stringent test for the accuracy of density functionals. As mentioned in Sec. III, the HTBH38 and NHTBH38 test sets established by Truhlar and coworkers^{48,49} will be used here to test the RPA-based functionals considered.

Our findings on barrier heights, *i.e.* activation energies (Fig. 3), are summarized in Table V. MEs and MUEs are calculated with respect to the best theoretical estimates currently available for HT and NHT barrier heights given in Refs. 48 and 49, respectively. Furthermore the MUREs in HT barriers [panel (a)] and NHT barriers [panel (b)] are depicted in Fig. 4. Note that legends given in Fig. 4 follow the color code used in Fig. 2. To establish a connection to Ref. 9, Tab. V also shows MEs and MUEs for the BH6 test set,⁹⁵ which has been introduced as a computationally less intensive, but statistically representative subset of HT/NHTBH38. However, we do not present a detailed discussion on BH6 here, but stress that errors in BH6 essentially follow the trends found for HT/NHTBH38.

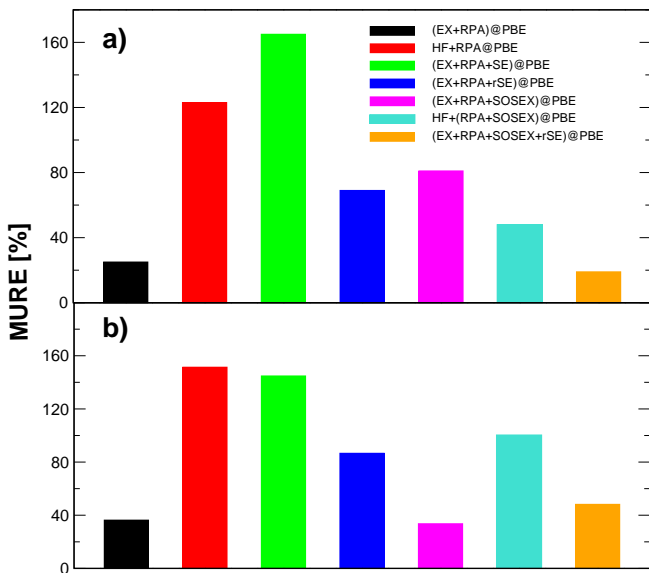


FIG. 4: Panel a) shows mean unsigned relative errors (MURE) in HT barrier heights of HTBH38. Panel b) shows MUREs in NHTBH38 for the RPA-based methods presented in this work. Energies use a cc-pV(T,Q)Z extrapolation and the frozen core approximation in calculated correlation energies.

One of the main findings of this work is the astonishingly good performance of the conventional (EX+RPA)@PBE scheme for activation energies. To be more specific, (EX+RPA)@PBE performs significantly better for the transfer of hydrogen atoms than for reac-

tions involving heavier atoms. For HTBH38, the ME obtained using (EX+RPA)@PBE amounts to -0.8 kJ/mol and the associated MUE amounts to 7.1 kJ/mol. These error margins are similar to those of some of the range-separated, generalized KS-DFT functionals like *e.g.* LC- ω PBE.¹¹⁰ The latter performs very well for chemical reaction barriers (see also Sec. IV D). However, for (EX+RPA)@PBE, the MUE increases by more than 50% when elements heavier than H, like *e.g.* F or Cl, are transferred. The MUE in NHTBH38 obtained using (EX+RPA)@PBE amounts to 12.1 kJ/mol together with a rather distinct underestimation of the barriers by -10.5 kJ/mol (ME).

On a relative scale, the MURE for HT reactions obtained using (EX+RPA)@PBE (see Fig. 4) amounts to approximately 20%, but increases to a value approximately twice as large for NHT reactions [panel (b)]. Note that reaction 7 in NHTBH38 has a barrier height of only -1.42 kJ/mol. For this reaction MUREs are extraordinarily large leading to an increase, which is seven to eight times as large as the corresponding value in HT reactions. The statistics would be drastically biased by such a case being very likely compensated by significantly extending the test set. Therefore, we decided to exclude reaction number 7 from the test set when calculating the MURE in NHTBH38.

Both HF+RPA@PBE and (EX+RPA+SE)@PBE show a strong underestimation of barriers with maximal errors as large as 50 kJ/mol. As mentioned above, the reason for this behavior has been attributed to small HOMO-LUMO differences found for some of the transition state structures, which are not correctly described by the simple (EX+RPA+SE)@PBE scheme. Indeed, the renormalization of SE alleviates the problem, and the corresponding ME and MUE in HTBH38 obtained using (EX+RPA+rSE)@PBE are improved by almost 60% compared to (EX+RPA+SE)@PBE. Note that numerical results given in Tab. V nicely reflect the trend induced by incorporation of SE effects in the correlation energy contribution, *i.e.* it partially takes care of the lack of self-consistency in the EX@PBE energy. However, the rSE corrects for the strong underestimation of barriers seen in HF+RPA@PBE and (EX+RPA+SE)@PBE, but qualitatively reflects the same trend compared to (EX+RPA)@PBE.

The performance of (EX+RPA+SOSEX)@PBE for barrier heights has already been tested by Paier *et al.* for the BH6 test set.⁹ This work extends the findings of Ref. 9 by discriminating HT and NHT reactions. (EX+RPA+SOSEX)@PBE is less accurate for HT barriers than (EX+RPA)@PBE as indicated by an MUE of about 22 kJ/mol compared to 7 kJ/mol. Quantitatively, (EX+RPA+SOSEX)@PBE on average overestimates barrier heights for HTBH38 by the aforementioned 22 kJ/mol. This is in perfect agreement with the errors found for the BH6 test set.⁹ On the other hand, (EX+RPA+SOSEX)@PBE performs substantially better for NHT barrier heights,

where ME and MUE are found to be close to the ones obtained using (EX+RPA)@PBE. On average, (EX+RPA+SOSEX)@PBE overestimates NHT barriers by approximately 13kJ/mol, whereas (EX+RPA)@PBE underestimates them by 11kJ/mol. As shown in Fig. 4, the MURE in NHT barriers obtained using (EX+RPA+SOSEX)@PBE amounts to 34% [panel (b) in Fig. 4] slightly outperforming (EX+RPA)@PBE by approximately 3%.

Incorporation of SE effects into (EX+RPA+SOSEX)@PBE in the hybrid fashion, *i.e.* HF+(RPA+SOSEX)@PBE, leads to very different results when applied to HT and NHT reactions, respectively. HF+(RPA+SOSEX)@PBE improves HT reaction barrier heights, whereas NHT barrier heights deteriorate appreciably compared to (EX+RPA+SOSEX)@PBE, ending up with an overall underestimation of barrier heights.

The situation becomes noticeably better, for both HT and NHT barrier heights, upon combination of explicitly computed renormalized SE with (EX+RPA+SOSEX)@PBE. Barrier heights obtained using (EX+RPA+SOSEX+rSE)@PBE are of similar quality as “conventional” (EX+RPA)@PBE, although the unsigned error in NHT test set is slightly larger. (EX+RPA+SOSEX+rSE)@PBE overestimates HT barriers by approximately 3.6kJ/mol, but reduces the ME in NHT barriers (ME = -6.3kJ/mol) compared to (EX+RPA)@PBE.

To summarize this section, SOSEX and rSE tend to overestimate and underestimate reaction barrier heights, respectively. Thus it appears advantageous to combine the correction schemes in order to achieve a partial error compensation. This mechanism works most efficiently for HT reactions and somewhat less so for NHT reactions. Taking the excellent performance of (EX+RPA+SOSEX+rSE)@PBE for binding energies (see previous Section) into account, this functional offers the most balanced description in terms of binding energies as well as activation energies.

C. Reaction energies in HTBH38 and NHTBH38

As shown in Fig. 3, knowing both forward (V_f^\ddagger) and reverse (V_r^\ddagger) reaction barrier heights, corresponding reaction energies ΔE are readily calculated using

$$\Delta E = V_f^\ddagger - V_r^\ddagger. \quad (21)$$

Note that 17 out of the 38 reactions contained in HTBH38 lead to a nonzero ΔE , whereas NHTBH38 comprises 13 reactions with a forward barrier different from the reverse barrier. The corresponding MEs and MUEs of the RPA-based functionals are compiled in Tab. VI, and the MUREs are depicted in Fig. 5

Similar to the trends found for atomization energies, HT reaction energies are significantly improved upon in-

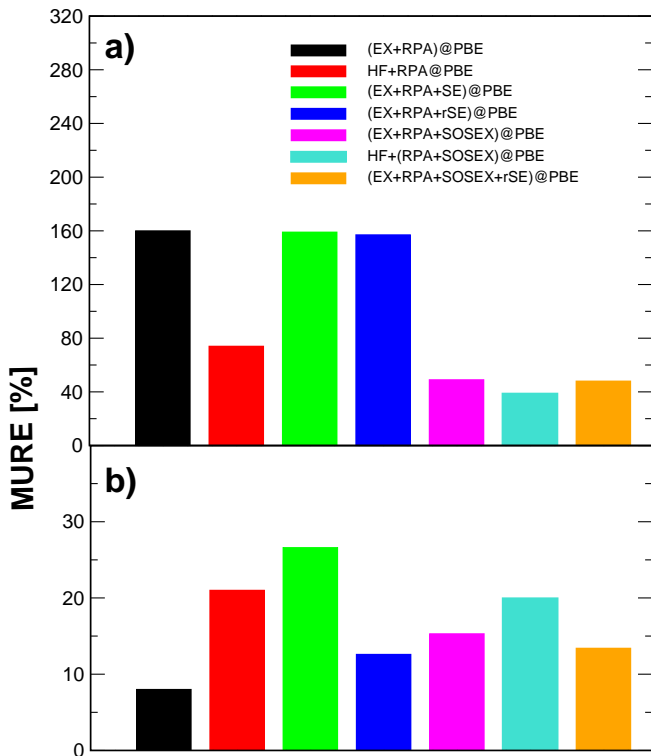


FIG. 5: Panel a) shows mean unsigned relative errors (MURE) in HT reaction energies of HTBH38. Panel b) shows MURE for the reaction energies of NHTBH38. Energies use a cc-pV(T,Q)Z extrapolation and the frozen core approximation to the correlation energies. Color code of legends follows Fig. 4.

clusion of (SOSEX)@PBE to (EX+RPA)@PBE as reflected in the MUEs. For (EX+RPA)@PBE the MUE in HT reactions amounts to 18.2kJ/mol and drops down to 4.6kJ/mol employing (EX+RPA+SOSEX)@PBE. Hence, it appears that eliminating the one-electron self-correlation error contained in RPA@PBE is beneficial for HT reaction energies. This is not entirely surprising, since the aforementioned error will be largest for breaking and creating covalent hydrogen bonds. For reactions involving heavier atoms, as exemplified by the reaction energies in NHTBH38, the correction due to (SOSEX)@PBE appears to perform less favorably. This can be seen by inspection of Fig. 5 presenting MUREs in HT [panel (a)] as well as NHT reaction energies [panel (b)]. For (EX+RPA)@PBE the MUE in NHTBH38 amounts to 9.7kJ/mol, which is rather low, whereas for NHT reaction energies obtained using (EX+RPA+SOSEX)@PBE, the MUE increases to 20.5kJ/mol.

Concerning effects due to SE@PBE and rSE@PBE to (EX+RPA)@PBE, no significant improvement of HT reaction energies over (EX+RPA)@PBE has been found. The MEs and MUEs given in Tab. VI for (EX+RPA+SE)@PBE (ME = -3 kJ/mol; MUE = 16.9 kJ/mol) and (EX+RPA+rSE)@PBE (ME = -2.9 kJ/mol; MUE = 17 kJ/mol) are essentially unaltered

TABLE VI: Mean errors and mean unsigned errors [kJ/mol] in the reaction energies obtained using calculated barrier heights of the HTBH38/04 hydrogen transfer as well as NHTBH38/04 non-hydrogen transfer barrier heights.

Method	HTBH38		NHTBH38	
	ME	MUE	ME	MUE
(EX+RPA)@PBE	-3.2	18.2	-7.8	9.7
HF+RPA@PBE	2.2	12.3	-1.6	14.4
(EX+RPA+SE)@PBE	-3.0	16.9	9.4	24.6
(EX+RPA+rSE)@PBE	-2.9	17.0	-1.2	11.8
(EX+RPA+SOSEX)@PBE	2.7	4.6	-18.4	20.5
HF+(RPA+SOSEX)@PBE	2.8	4.1	-12.2	15.7
(EX+RPA+SOSEX+rSE)@PBE	3.0	4.4	-11.9	15.5

compared to (EX+RPA)@PBE. In contrast to HT, the rSE correction helps to improve the NHTBH38 reaction energies and alleviates the overestimation found for simple (EX+RPA+SE)@PBE drastically (ME = -1.2 kJ/mol compared to 9.4 kJ/mol). The associated MUE as well as MURE decrease by approximately 50%.

We now turn to a discussion of results obtained using the “hybrid variants”, which employ the HF energy as the reference energy on the EX level. Specifically for (EX+RPA)@PBE, HT reaction energies are substantially improved upon replacement of EX@PBE through HF. As can be seen from Tab. VI, the MUE is reduced by approximately 6kJ/mol, which translate into an improvement of the MURE by approximately 50%. HT reaction energies obtained using (EX+RPA+SOSEX)@PBE, which are fairly accurate, are hardly affected by changing to the corresponding hybrid scheme. Employing HF+(RPA+SOSEX)@PBE, however, the MUE in NHT reaction energies is reduced by 5kJ/mol. In addition, the ME amounts to -12kJ/mol, which compares very favorably to the ME of -18kJ/mol obtained using (EX+RPA+SOSEX)@PBE. In terms of performance, the combined scheme (EX+RPA+SOSEX+rSE)@PBE is on par with HF+(RPA+SOSEX)@PBE for both HTBH38 and NHTBH38 reaction energies. (EX+RPA+SOSEX+rSE)@PBE has two apparent favorable features: (i) it substantially improves HT reaction energies obtained using (EX+RPA)@PBE, and (ii) it performs approximately similarly well for *all* of the test sets investigated in this work. In other words, the overall variation in error margins for atomization energies, barrier heights, and reaction energies is smallest for (EX+RPA+SOSEX+rSE)@PBE lending the functional robustness. Among the functionals discussed in this work, (EX+RPA)@PBE performs best for NHT reaction energies. Nevertheless, (EX+RPA+SOSEX+rSE)@PBE performs only slightly worse, but given the better HT reaction barrier heights and the significantly better reaction energies in HTBH38, (EX+RPA+SOSEX+rSE)@PBE is among the RPA-based functionals tested in this work, the functional of broadest applicability.

D. Comparing RPA to semilocal and hybrid functionals

To close the discussion on the performance of the RPA- and RPA+SOSEX-based functionals, we briefly compare molecular atomization and activation energies to results obtained using commonly applied semilocal as well as HF/DFT hybrid functionals. To render direct comparisons easier, Table VII repeats MUEs for G2-1, BH6, HTBH38, and NHTBH38 for three of the RPA-based functionals, which perform best, namely (EX+RPA)@PBE, HF+(RPA+SOSEX)@PBE, and (EX+RPA+SOSEX+rSE)@PBE. The above mentioned statistical errors are compared to PBE-GGA, BLYP-GGA^{113,114} as well as the PBE0^{111,115} and B3LYP¹¹⁶ global hybrid functionals. In addition, we also present results obtained using the above mentioned LC- ω PBE range-separated hybrid functional.¹¹⁰ LC- ω PBE mixes a fraction of EX at the long-range of the Coulomb interaction (for definitions, see Ref. 110), but uses only one parameter (0.40 bohr⁻¹) for defining a universal range separation. It is remarkable that LC- ω PBE describes reaction barriers and atomization energies extremely accurately representing a landmark among hybrids for thermochemistry and kinetics. Admittedly, for extended systems admixture of EX on the long-range is detrimental and leads to *e.g.* strongly overestimated band gaps.¹¹⁷

Returning to RPA, activation energies obtained using (EX+RPA)@PBE are *de facto* on par with LC- ω PBE (Tab. VII). Trends for GGA and global hybrid functionals like PBE0 or B3LYP are rather general, hence other GGA-type and global hybrid functionals perform quite similarly (for other functionals, see *e.g.* Ref. 112). Although, HF+(RPA+SOSEX)@PBE does not perform as well as (EX+RPA)@PBE for activation energies of non-hydrogen transfer reactions (corresponding MUE is almost twice as large), it performs certainly better than PBE and BLYP. HF+(RPA+SOSEX)@PBE is only slightly outperformed by B3LYP for the aforementioned activation energies in NHTBH38. According to this synopsis, (EX+RPA+SOSEX+rSE)@PBE certainly shows the most balanced description of molecular binding and

TABLE VII: Comparing the three best-performing functionals presented in Tab. V to widely used semilocal and HF/DFT hybrid functionals. Mean unsigned errors in individual test sets are given in kJ/mol.

Method	G2-1	BH6	HTBH38	NHTBH38
(EX+RPA)@PBE	42.8 ^a	7.5 ^a	7.1	12.1
HF+(RPA+SOSEX)@PBE	13.0	9.2	13.8	25.5
(EX+RPA+SOSEX+rSE)@PBE	13.9	3.7	5.4	17.6
PBE	36.0 ^b	38.9 ^c	39.0 ^d	33.9 ^d
BLYP	19.7 ^b	32.6 ^c	31.5 ^d	36.4 ^d
PBE0	14.6 ^b	19.2 ^c	17.7 ^d	14.1 ^d
B3LYP	10.0 ^b	19.7 ^c	17.7 ^d	18.2 ^d
LC- ω PBE	15.6 ^e		5.4 ^e	10.0 ^e

^a See Ref. 9. Note that differences in the MUE of G2-1 are due to the different values for the experimental dissociation energies (see Ref. 108).

^b Ref. 111

^c Ref. 112

^d Ref. 49

^e Ref. 110. Note that the MUE given here for G2 refers to G2-2 comprising 148 molecules. The MUE for G2-1 will be lower.

barrier heights. It performs similarly well as hybrid functionals in terms of atomization energies, outperforms both GGA and hybrid functionals in terms of hydrogen-transfer barrier heights, and performs equivalently well for non-hydrogen barrier heights as aforementioned hybrids do.

Although, this work is not devoted to weak, van-der-Waals-type of interactions, it should be emphasized that all of the RPA-based functionals presented here do include them seamlessly as already mentioned in the introduction. It is well known that neither GGA nor hybrid functionals do show the correct van der Waals asymptote.

V. CONCLUSIONS

In summary, we have reported an extensive assessment of several exact-exchange based post-KS density functionals involving RPA correlation energies and beyond. Correlation energies have been assessed for solids as well as for small molecules. Specifically we calculated atomization energies of solids and molecules using (EX+RPA)@PBE, (EX+RPA+SOSEX)@PBE as well as HF+RPA@PBE and HF+(RPA+SOSEX)@PBE, where the latter approach gives binding energies improved by approximately 50% compared to “conventional” (EX+RPA)@PBE. Furthermore, we investigated the performance of individual functionals for chemical reaction barrier heights or activation energies em-

ploying large and well established test sets. Generally, we found that it is rather difficult to systematically improve on (EX+RPA)@PBE reaction barrier heights, although modest improvements using (EX+RPA+SOSEX+rSE)@PBE were achieved for HT barriers. Importantly, the favorable impact of the correlation energy contribution stemming from SE effects on binding energies does not translate to reaction barriers. This has been explained by divergent correlation energy contributions in systems with small HOMO-LUMO gaps. Therefore, application of “SE” to systems with small one-electron band gaps is not possible, but a renormalization of “SE” helps to alleviate the problem. Surprisingly, (EX+RPA)@PBE yields reaction energies of high accuracy for reactions involving non-hydrogen atoms. Good and robust performance of a novel RPA-based functional (EX+RPA+SOSEX+rSE)@PBE is a central finding of this work. It improves on binding or atomization energies compared to (EX+RPA)@PBE, improves on HT barrier heights as well as reaction energies.

Acknowledgements

This work was supported by the Austrian Fonds zur Förderung der wissenschaftlichen Forschung (FWF) within SFB ViCom (F41). The work at Rice University was supported by the US Department of Energy (Grant No. DE-FG02-09ER16053) and The Welch Foundation (C-0036).

¹ D. Bohm and D. Pines, Phys. Rev. **92**, 609 (1953).

² M. Gell-Mann and K. A. Brueckner, Phys. Rev. **106**, 364

(1957).

³ F. Furche, Phys. Rev. B **64**, 195120 (2001).

- ⁴ M. Fuchs and X. Gonze, Phys. Rev. B **65**, 235109 (2002).
- ⁵ F. Furche and T. Van Voorhis, J. Chem. Phys. **122**, 164106 (2005).
- ⁶ G. E. Scuseria, T. M. Henderson, and D. C. Sorensen, J. Chem. Phys. **129**, 231101 (2008).
- ⁷ B. G. Janesko, T. M. Henderson, and G. E. Scuseria, J. Chem. Phys. **130**, 081105 (2009).
- ⁸ J. Toulouse, I. C. Gerber, G. Jansen, A. Savin, J. G. Ángyán, Phys. Rev. Lett. **102**, 096404 (2009).
- ⁹ J. Paier, B. G. Janesko, T. M. Henderson, G. E. Scuseria, A. Grüneis, and G. Kresse, J. Chem. Phys. **132**, 094103 (2010), Erratum: *ibid.* **133**, 179902 (2010).
- ¹⁰ A. Marini, P. García-González, and A. Rubio, Phys. Rev. Lett **96**, 136404 (2006).
- ¹¹ H. Jiang and E. Engel, J. Chem. Phys **127**, 184108 (2007).
- ¹² J. Harl and G. Kresse, Phys. Rev. B **77**, 045136 (2008).
- ¹³ J. Harl and G. Kresse, Phys. Rev. Lett. **103**, 056401 (2009).
- ¹⁴ D. Lu, Y. Li, D. Rocca, and G. Galli, Phys. Rev. Lett. **102**, 206411 (2009).
- ¹⁵ J. F. Dobson and J. Wang, Phys. Rev. Lett **82**, 2123 (1999).
- ¹⁶ M. Rohlfing and T. Bredow, Phys. Rev. Lett **101**, 266106 (2008).
- ¹⁷ X. Ren, P. Rinke, and M. Scheffler, Phys. Rev. B **80**, 045402 (2009).
- ¹⁸ L. Schimka, J. Harl, A. Stroppa, A. Grüneis, M. Marsman, F. Mittendorfer, and G. Kresse, Nature Materials **9**, 741 (2010).
- ¹⁹ W. Zhu, J. Toulouse, A. Savin, and J. G. Ángyán, J. Chem. Phys. **132**, 244108 (2010).
- ²⁰ S. Lebègue, J. Harl, T. Gould, J. G. Ángyán, G. Kresse, and J. F. Dobson, Phys. Rev. Lett. **105**, 196401 (2010).
- ²¹ H. Eshuis, J. Yarkony, and F. Furche, J. Chem. Phys. **132**, 234114 (2010).
- ²² S. Ismail-Beigi, Phys. Rev. B **81**, 195126 (2010).
- ²³ F. Göttl and J. Hafner, J. Chem. Phys. **134**, 064102 (2011).
- ²⁴ H. Eshuis and F. Furche, J. Phys. Chem. Lett. **2**, 983 (2011).
- ²⁵ X. Ren, A. Tkatchenko, P. Rinke, and M. Scheffler, Phys. Rev. Lett. **106**, 153003 (2011).
- ²⁶ A. Heßelmann and A. Görling, Phys. Rev. Lett. **106**, 093001 (2011).
- ²⁷ A. Heßelmann and A. Görling, Mol. Phys. **109**, 2473 (2011).
- ²⁸ A. Ruzsinszky, J. P. Perdew, and G. I. Csonka, J. Chem. Phys. **134**, 114110 (2011).
- ²⁹ A. Heßelmann, J. Chem. Phys. **134**, 204107 (2011).
- ³⁰ W. Klopper, A. M. Teale, S. Coriani, T. B. Pedersen, and T. Helgaker, Chem. Phys. Lett. **510**, 147 (2011).
- ³¹ J. F. Dobson, in *Topics in Condensed Matter Physics*, edited by M. P. Das, Nova, New York, 1994.
- ³² C. Møller and M. S. Plesset, Phys. Rev. **46**, 618 (1934).
- ³³ A. D. Becke, J. Chem. Phys. **98**, 1372 (1993).
- ³⁴ A. D. Becke, J. Chem. Phys. **98**, 5648 (1993).
- ³⁵ J. P. Perdew, M. Ernzerhof, and K. Burke, J. Chem. Phys. **105**, 9982 (1996).
- ³⁶ D. L. Freeman, Phys. Rev. B **15**, 5512 (1977).
- ³⁷ A. Grüneis, M. Marsman, J. Harl, L. Schimka, and G. Kresse, J. Chem. Phys. **131**, 154115 (2009).
- ³⁸ J. Harl, L. Schimka, and G. Kresse, Phys. Rev. B **81**, 115126 (2010).
- ³⁹ T. M. Henderson and G. E. Scuseria, Mol. Phys. **108**, 2511 (2010).
- ⁴⁰ A. Ruzsinszky, J. P. Perdew, G. I. Csonka, O. A. Vydrov, and G. E. Scuseria, J. Chem. Phys. **125**, 194112 (2006).
- ⁴¹ P. Mori-Sánchez and A. J. Cohen, J. Chem. Phys. **125**, 201102 (2006).
- ⁴² C. D. Hu and D. C. Langreth, Phys. Rev. B **33**, 943 (1986).
- ⁴³ G. Kresse and A. Grüneis, unpublished results, October 3 (2008), presented at the XIV ESCMQC, Isola d'Elba, Italy.
- ⁴⁴ L. A. Curtiss, K. Raghavachari, P. Redfern, and J. Pople, J. Chem. Phys. **106**, 1063 (1997).
- ⁴⁵ J. A. Pople, M. Head-Gordon, D. J. Fox, K. Raghavachari, and L. A. Curtiss, J. Chem. Phys. **90**, 5622 (1989).
- ⁴⁶ L. A. Curtiss, C. Jones, G. W. Trucks, K. Raghavachari, and J. A. Pople, J. Chem. Phys. **93**, 2537 (1989).
- ⁴⁷ L. A. Curtiss, P. C. Redfern, K. Raghavachari, and J. A. Pople, J. Chem. Phys. **109**, 42 (1998).
- ⁴⁸ Y. Zhao, B. J. Lynch, and D. G. Truhlar, J. Phys. Chem. A **108**, 2715 (2004).
- ⁴⁹ Y. Zhao, N. González-García, and D. G. Truhlar, J. Phys. Chem. A **109**, 2012 (2005), **110**, 4942(E) (2006).
- ⁵⁰ B. G. Janesko and G. E. Scuseria, J. Chem. Phys. **128**, 244112 (2008).
- ⁵¹ A. Seidl, A. Görling, P. Vogl, J. A. Majewski, and M. Levy, Phys. Rev. B **53**, 3764 (1996).
- ⁵² R. T. Sharp and G. K. Horton, Phys. Rev. **90**, 317 (1953).
- ⁵³ J. D. Talman and W. F. Shadwick, Phys. Rev. A **14**, 36 (1976).
- ⁵⁴ M. E. Casida, Phys. Rev. A **51**, 2005 (1995).
- ⁵⁵ A. Szabo and N. S. Ostlund, *Modern Quantum Chemistry*, Dover, Mineola, New York, 1st edition, 1996.
- ⁵⁶ R. M. Dreizler and E. K. U. Gross, *Density Functional Theory*, Plenum Press, New York, 1995.
- ⁵⁷ R. W. Godby, M. Schlüter, and L. J. Sham, Phys. Rev. Lett. **56**, 2415 (1986).
- ⁵⁸ R. W. Godby, M. Schlüter, and L. J. Sham, Phys. Rev. B **37**, 10159 (1988).
- ⁵⁹ T. Kotani, J. Phys.: Condens. Matter **10**, 9241 (1998).
- ⁶⁰ M. Grüning, A. Marini, and A. Rubio, Phys. Rev. B **R74**, 161103 (2006).
- ⁶¹ M. Hellgren and U. von Barth, Phys. Rev. B **76**, 075107 (2007).
- ⁶² M. Hellgren, D. R. Rohr, and E. K. U. Gross, J. Chem. Phys. **136**, 034106 (2012).
- ⁶³ D. C. Langreth and J. P. Perdew, Solid. State. Commun. **17**, 1425 (1975).
- ⁶⁴ O. Gunnarsson and B. I. Lundqvist, Phys. Rev. B **13**, 4274 (1976).
- ⁶⁵ D. C. Langreth and J. P. Perdew, Phys. Rev. B **15**, 2884 (1977).
- ⁶⁶ E. K. U. Gross and W. Kohn, Phys. Rev. Lett. **55**, 2850 (1985).
- ⁶⁷ G. Onida, L. Reining, and A. Rubio, Rev. Mod. Phys. **74**, 601 (2002).
- ⁶⁸ F. E. Harris, H. J. Monkhorst, and D. L. Freeman, *Algebraic and Diagrammatic Methods in Many-Fermion Theory*, Oxford University Press, New York, Oxford, 1992.
- ⁶⁹ B. H. Brandow, Rev. Mod. Phys. **39**, 771 (1967).
- ⁷⁰ R. J. Bartlett and M. Musiał, Rev. Mod. Phys. **79**, 291 (2007).
- ⁷¹ H. Kümmel, K. H. Lührmann, and J. G. Zabolitzky, Phys. Rep. **36**, 1 (1978).

- ⁷² R. F. Bishop and K. H. Lührmann, *Phys. Rev. B* **17**, 3757 (1978).
- ⁷³ R. F. Bishop and K. H. Lührmann, *Phys. Rev. B* **26**, 5523 (1982).
- ⁷⁴ J. Čížek, *J. Chem. Phys.* **45**, 4256 (1966).
- ⁷⁵ J. Čížek, *Adv. Chem. Phys.* **14**, 35 (1969).
- ⁷⁶ J. Paldus, J. Čížek, and I. Shavitt, *Phys. Rev. A* **5**, 50 (1972).
- ⁷⁷ R. J. Bartlett and G. D. Purvis III, *Int. J. Quantum Chem.* **14**, 561 (1978).
- ⁷⁸ R. J. Bartlett, *Ann. Rev. Phys. Chem.* **32**, 359 (1981).
- ⁷⁹ L. Hedin, *Phys. Rev.* **139**, A796 (1965).
- ⁸⁰ P. Nozières and D. Pines, *Nuovo Cimento* **9**, 470 (1958).
- ⁸¹ H. J. Monkhorst and J. Oddershede, *Phys. Rev. Lett.* **30**, 797 (1973).
- ⁸² G. Jansen, R.-F. Liu, and J. G. Ángyán *J. Chem. Phys.* **133**, 154106 (2010).
- ⁸³ A. Görling and M. Levy *Phys. Rev. B* **47**, 131105 (1993).
- ⁸⁴ R. C. Raffenetti, K. Ruedenberg, C. L. Janssen, and H. F. Schaefer, *Theor. Chim. Acta* **86**, 149 (1992).
- ⁸⁵ K. Ruedenberg, L. M. Cheung, and S. T. Elbert, *Int. J. Quantum. Chem.* **16**, 1069 (1976).
- ⁸⁶ G. E. Scuseria and H. F. Schaefer, *Chem. Phys. Lett.* **142**, 354 (1987).
- ⁸⁷ J. P. Perdew, K. Burke, and M. Ernzerhof, *Phys. Rev. Lett.* **77**, 3865 (1996), (E) *ibid.* **78**, 1396 (1997).
- ⁸⁸ H. Eshuis, J. E. Bates, and F. Furche, *Theor. Chem. Acc.* **131**, 1084 (2012).
- ⁸⁹ G. Kresse and J. Hafner, *Phys. Rev. B* **48**, 13115 (1993).
- ⁹⁰ G. Kresse and J. Furthmüller, *Phys. Rev. B* **54**, 11169 (1996).
- ⁹¹ G. Kresse and J. Furthmüller, *Comput. Mater. Sci.* **6**, 15 (1996).
- ⁹² Gaussian Development Version, Revision G.01, M. J. Frisch, G. W. Trucks, H. B. Schlegel *et. al.*, Gaussian, Inc., Wallingford CT, 2007.
- ⁹³ V. Blum, R. Gehrke, F. Hanke, P. Havu, V. Havu, X. Ren, K. Reuter, and M. Scheffler *Comput. Phys. Commun.* **180**, 2175 (2009).
- ⁹⁴ X. Ren, P. Rinke, V. Blum, J. Wieferink, A. Tkatchenko, A. Sanfilippo, K. Reuter, and M. Scheffler, to be published.
- ⁹⁵ B. J. Lynch and D. G. Truhlar, *J. Phys. Chem. A* **107**, 8996 (2003), **108**, 1460(E) (2004).
- ⁹⁶ W. Kutzelnigg and J. D. Morgan III, *J. Chem. Phys.* **96**, 4484 (1992).
- ⁹⁷ T. Helgaker, W. Klopper, H. Koch, and J. Noga, *J. Chem. Phys.* **106**, 9639 (1997).
- ⁹⁸ A. Halkier, T. Helgaker, P. Jørgensen, W. Klopper, H. Koch, J. Olsen, and A. K. Wilson, *Chem. Phys. Lett.* **286**, 243 (1998).
- ⁹⁹ T. H. Dunning, Jr., *J. Chem. Phys.* **90**, 1007 (1989).
- ¹⁰⁰ D. E. Woon and T. H. Dunning, Jr., *J. Chem. Phys.* **98**, 1358 (1993).
- ¹⁰¹ S. F. Boys and F. Bernardi, *Mol. Phys.* **19**, 553 (1970).
- ¹⁰² A. Grüneis, M. Marsman, and G. Kresse, *J. Chem. Phys.* **133**, 074107 (2010).
- ¹⁰³ V. N. Staroverov, G. E. Scuseria, J. Tao, and J. P. Perdew, *Phys. Rev. B* **69**, 075102 (2004).
- ¹⁰⁴ O. Madelung, *Semiconductors: Data Handbook*, Springer, Berlin, 3rd edition, 2004.
- ¹⁰⁵ S. Trampert, O. Brandt, and K. Ploog, *Semiconductors and Semimetals*, volume 50, chapter Crystal Structure of Group III Nitrides, Academic, San Diego, 1998, edited by J. I. Pankove and T. D. Moustakas.
- ¹⁰⁶ D. K. Smith and H. R. Leider, *J. Appl. Cryst.* **1**, 246 (1968).
- ¹⁰⁷ A. Grüneis, G. H. Booth, M. Marsman, J. Spencer, A. Alavi, and G. Kresse, *J. Chem. Theory Comput.* **7**, 2780 (2011).
- ¹⁰⁸ D. Feller and K. A. Peterson, *J. Chem. Phys.* **110**, 8384 (1999).
- ¹⁰⁹ L. Schimka, J. Harl, and G. Kresse, *J. Chem. Phys.* **134**, 024116 (2011).
- ¹¹⁰ O. Vydrov and G. E. Scuseria, *J. Chem. Phys.* **125**, 234109 (2006).
- ¹¹¹ M. Ernzerhof and G. E. Scuseria, *J. Chem. Phys.* **110**, 5029 (1999).
- ¹¹² K. Yang, J. Zheng, Y. Zhao, and D. G. Truhlar, *J. Chem. Phys.* **132**, 164117 (2010).
- ¹¹³ A. D. Becke, *Phys. Rev. A* **38**, 3098 (1988).
- ¹¹⁴ C. Lee, W. Yang, and R. G. Parr, *Phys. Rev. B* **37**, 785 (1988).
- ¹¹⁵ C. Adamo and V. Barone, *J. Chem. Phys.* **110**, 6158 (1999).
- ¹¹⁶ P. J. Stephens, F. J. Devlin, C. F. Chabalowski, and M. J. Frisch, *J. Phys. Chem.* **98**, 11623 (1994).
- ¹¹⁷ I. C. Gerber, J. G. Ángyán, M. Marsman, and G. Kresse, *J. Chem. Phys.* **127**, 054101 (2007).